Electron affinity of atomic scandium and yttrium and excited states of their negative ions

Rui Zhang, Yuzhu Lu, Rulin Tang, et al.

View Online   **Export Citation**   **CrossMark**

ARTICLES YOU MAY BE INTERESTED IN

Electron affinity of atomic scandium and yttrium and excited states of their negative ions

Rui Zhang, [ID] Yuzhu Lu, Rulin Tang, and Chuangang Ning[a] [ID]

AFFILIATIONS

Department of Physics, State Key Laboratory of Low Dimensional Quantum Physics, Frontier Science Center for Quantum Information, Tsinghua University, Beijing 100084, China

[a]Author to whom correspondence should be addressed: ningcg@tsinghua.edu.cn

ABSTRACT

The latest experimental electron affinity (EA) values of atomic scandium and yttrium were 0.189(20) and 0.308(12) eV as reported by Feigerle *et al.* in 1981. The measurement accuracy of these was far lower than that of other transition elements, and no conclusive result had been made on the excited states of their negative ions. In the current work, we report more accurate EA values of Sc and Y and the electronic structure of their negative ions using the slow-electron velocity-map imaging method. The EA values of Sc and Y are determined to be 0.179 378(22) and 0.311 29(22) eV, respectively. The ground state of Sc^- is identified as $3d4s^24p\ ^1D_2$, and the ground state is $4d5s^25p\ ^1D_2$ for Y^-. Furthermore, several excited states of Sc^- and Y^- are observed: Sc^- ($^3D_1$) and Y^- ($^3D_1$, $^3D_2$, $^3D_3$, $^3F_2$, and $^3F_3$), and their energy levels are determined to be 1131.8(28), 1210.0(13), 1362.3(30), 1467.7(26), 1747(16), and 1987(33) cm^{-1}, respectively.

Published under an exclusive license by AIP Publishing. https://doi.org/10.1063/5.0124882

I. INTRODUCTION

Negative ions play significant roles in atomic and molecular physics.[1,2] To understand the properties of negative ions, it is crucial to measure their electronic structures and to determine electron affinity (EA) values.[3] Measurements of EAs for most elements in the Periodic Table have steadily improved over the last 50 years.[4–7] Most of them have an accuracy typically better than 0.1 meV. Sc and Y are the last two non-radioactive transition elements whose EAs have not been accurately measured.[7] Moreover, no definitive conclusion for the excited states of Sc^- and Y^- has been made due to the extremely complicated photoelectron energy spectra and the contamination from their hydride anions ScH^- and YH^- since the work by Feigerle *et al.* in 1981.[8]

Scandium (Sc, atomic number Z = 21) is the first transition element in the Periodic Table. For a very long time, it was thought that the extra electron of Sc^- filled in the d orbital like that of other transition group atomic anions. In 1981, Feigerle *et al.* conducted the first measurement of the EA value of atomic Sc via the laser photoelectron electron spectroscopy (LPES) method at a wavelength of 488 nm and pointed out that the extra electron was filled in the p orbital.[8] They obtained EA(Sc) = 0.189 ± 0.020 eV and another bound excited state with a binding energy of 0.042 ± 0.020 eV. The

configuration of these two bound states of Sc^- was determined to be $3d4s^24p$ based on the selection rules of photodetachment. However, they could not conclude which of the two terms, ^1D and ^3D, was the ground state and which was the excited state lying 0.15 eV higher. Since then, there was no further reported experiment to study the electronic structure of Sc^-. On the theoretical side, Jeung *et al.* in 1985 calculated the three lowest energy states of Sc^- using the full configuration-interaction (CI) method and compared them with the energy of the neutral ground state $(3d4s^2)\ ^2D$ of Sc.[9] Their results showed that the ground state of Sc^- was $(3d4s^24p)\ ^1D$ and the EA value was 0.14 eV. The remaining two possible configurations $(3d^24s^2)\ ^3F$ and $(3d4s^24p)\ ^3D$ were not bound states with energies of 0.55 and 0.02 eV higher than the ground state of the neutral Sc, respectively. In 1987, Fischer *et al.* obtained EA(Sc) = 0.152 eV using the multiconfiguration Hartree–Fock theory.[10] They also presented a simple explanation of why the extra electron of Sc^- occupies the $4p$ orbital instead of the $3d$ orbital: the less overlap of the $4p$ orbital with the $4s$ and $3d$ orbitals reduces the Coulomb repulsion. In 1988, Bauschlicher *et al.* suggested both ^1D and ^3D of Sc^- were bound states with binding energies of 0.195 and 0.011 eV, respectively, using second-order CI (SOCI) calculations.[11] In 1998, Miura *et al.* added the correction of relativistic effects in their calculations and obtained the binding energies of ^1D and ^3D of Sc^- being

0.181 and 0.050 eV,[12] respectively, which were in good agreement with the experimental values of Feigerle *et al.*

Yttrium (Y, atomic number Z = 39) is a heavier congener of scandium. The only experimental report on the measurement of the EA(Y) value also comes from the work of Feigerle *et al.* in 1981 using the LPES method.[8] They observed two definite bound states (^1D and ^3D) and a suspected excited bound state (^3F). Like Sc, the extra electron of Y^- was filled in the p orbital, and the two observed bound states were assigned to the electronic configuration of $4d5s^25p$. The binding energies of ground state ^1D and excited state ^3D were determined to be 0.308 ± 0.012 and 0.165 ± 0.025 eV, respectively. There is no further experiment to study the electronic structure of Y^-. On the theoretical side, Bauschlicher *et al.* calculated the binding energies of three possible bound states (^1D, ^3F, ^3D) as 0.398, 0.179, and 0.103 eV via the SOCI calculations in 1989.[11]

In the present work, we try to measure the electronic structures of Sc^- and Y^- utilizing the slow-electron velocity-map imaging (SEVI) and cold-ion trap method.[13–15] SEVI has a very high energy resolution, typically a few cm^{-1} for low-energy electrons,[15–17] and the ability to selectively quench excited states via collisions in the cold ion trap makes this method a powerful tool for investigating the complicated spectra of atomic anions. Our group has successfully utilized this method to measure the EA values of many transition elements,[15,18–27] lanthanides,[28–31] and actinides,[32–34] with an accuracy of about 0.1 meV. Recently, we further extended the tuning range of our laser system into the infrared band for resolving complicated energy spectra. As demonstrated in our previous work for Ta^-, this extension is crucial for resolving complicated energy spectra of elements with very low EA values.[22] At lower photon energy, fewer photodetachment channels are opened, and the energy resolution of SEVI (ΔE) improves because it is proportional to the square root of the kinetic energy of photoelectrons (E_k), i.e., $\Delta E \propto \sqrt{E_k}$. Thus, the lower the kinetic energy, the higher the energy resolution and the less the overlap between neighboring photodetachment channels.
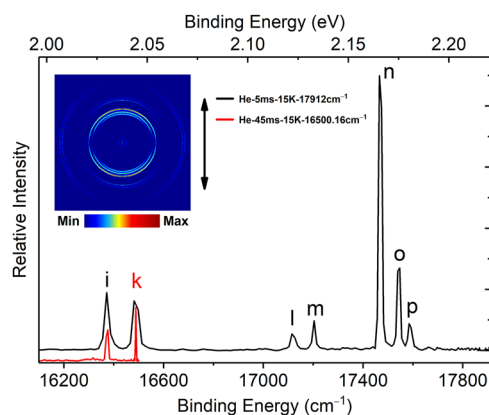

FIG. 2. (a) The red solid line shows the linear least squares fitting of the photon energy $h\nu$ and the photoelectron spherical shell's squared radius r^2, and its intercept, 16 488.70(18) cm^{-1}, is the binding energy of transition k. (b) The binding energy (BE) of the photodetachment channel Sc($^2F_{7/2}$) ← Sc$^-$($^1D_2$) as a function of the photoelectron kinetic energy. The green dashed lines represent ± 0.18 cm^{-1} uncertainty.

II. EXPERIMENTAL METHODS

The details of our SEVI apparatus have been described elsewhere previously.[15,19,25] It has four main components: the laser ablation ion source, the cryogenic ion trap, the time-of-flight (TOF) mass spectrometer, and the SEVI system. Anions are generated by

FIG. 1. The photoelectron image and spectra of Sc^- observed at the photon energies of 17 912 cm^{-1} in black and 16 500.16 cm^{-1} in red. The latter is 10 cm^{-1} above the photodetachment threshold of transition k. The direction of the laser polarization is indicated by the double-headed arrow.
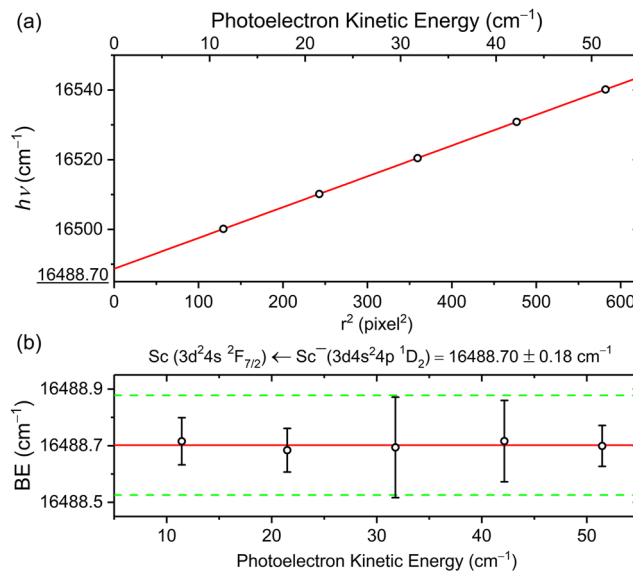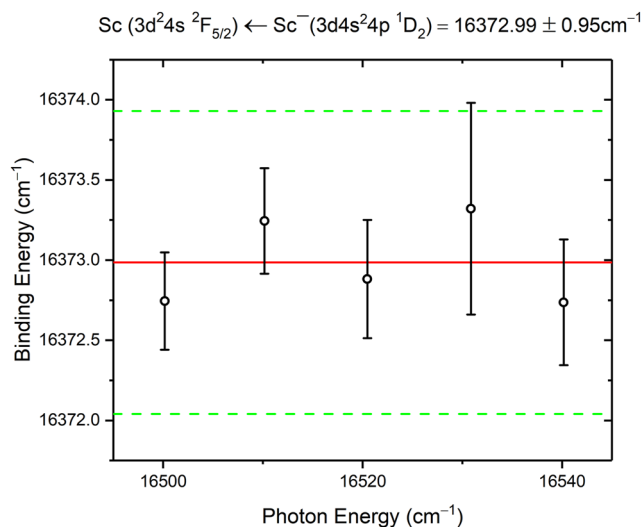

FIG. 3. The binding energy (BE) of the photodetachment channel Sc($^2F_{5/2}$) ← Sc$^-$($^1D_2$) as a function of the photon energy $h\nu$.
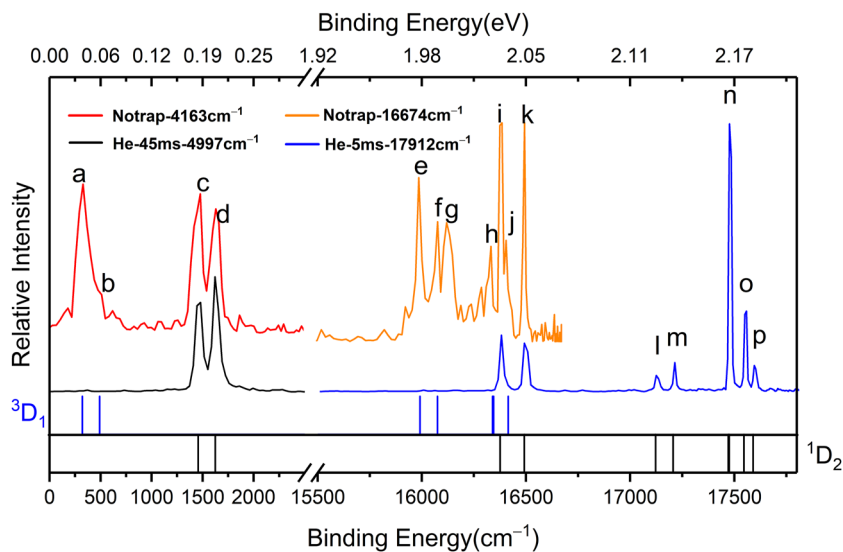
FIG. 4. The photoelectron energy spectra of Sc⁻ measured at different photon energies. The upper and lower curves show the comparison of measurements in the ion-trap-off and the ion-trap-on mode. Sc⁻ ions are trapped with He as the buffer gas to observe the anionic ground state in the ion-trap-on mode. In addition, the short-lived excited states can be observed by turning off the ion trap. There are two sets of sticks below the spectra indicating the energy levels of the final neutral states. The black sticks are for the anionic ground state $^1D_2$, and the blue sticks are for the excited state $^3D_1$.
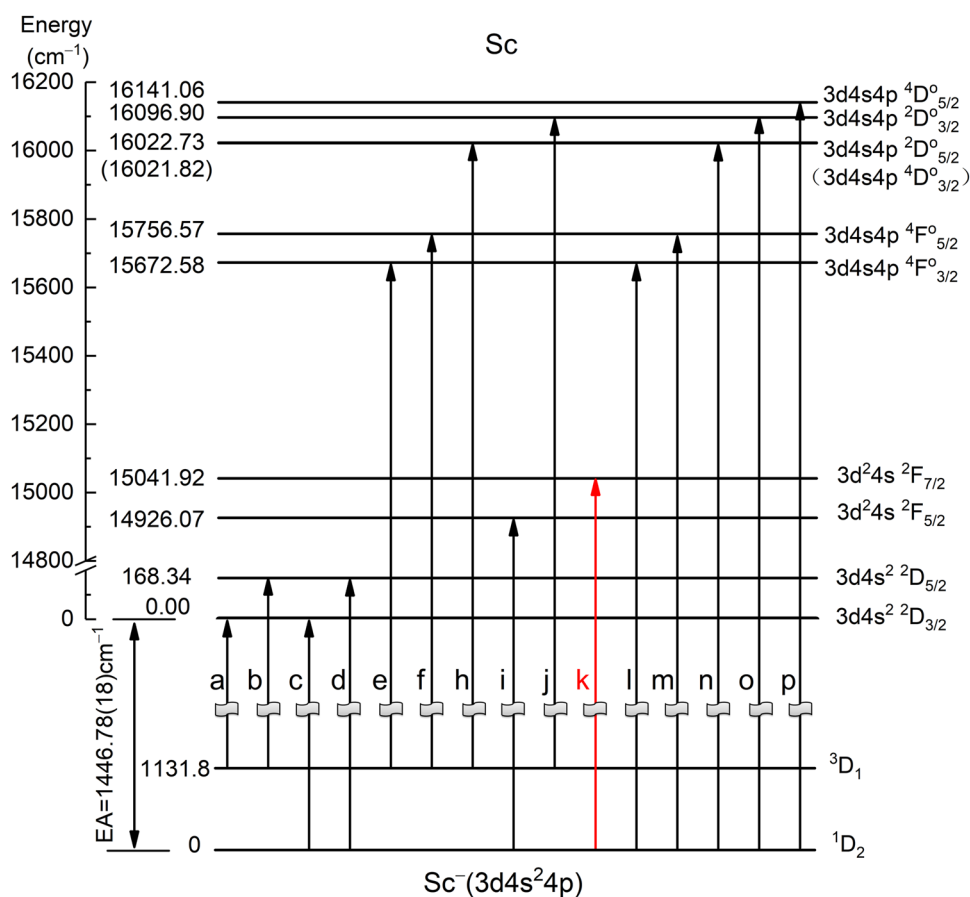
FIG. 5. The relative energy levels of Sc⁻ and Sc based on current measurements. The ground state of Sc is $3d4s^2$ $^2D_{3/2}$, and the ground state is $3d4s^24p$ $^1D_2$ for Sc⁻. The transition labels are the same as the indices of measured peaks in Fig. 2. The transition $k(^1D_2 \rightarrow {}^2F_{7/2})$ in red is selected for the electron affinity measurement of Sc in the present work.

focusing a pulsed 532-nm Nd:YAG laser beam onto the metal targets and are then accumulated in a radio frequency (RF) octupole ion trap that is installed on a cold head.[35] The trapped anions deplete their kinetic energies via the collisions with the butter gas (usually H_2 or He). The excited states of anions can be selectively quenched by choosing the buffer gas or changing the trap time, and H_2 is usually more effective to quench excited states than He. This feature is very helpful for the spectrum assignment. The trapped ions can be ejected out and analyzed in a Wiley–McLaren type time-of-flight (TOF) mass spectrometer.[36] To observe short-lived excited states, the ion trap can be turned off and let the ions directly pass through the ion trap. The anions of interest are then photodetached by a tunable laser, and the photoelectrons are analyzed via a velocity-map imaging (VMI) spectrometer.[17,37] The photoelectron distribution can be reconstructed from the projected image via an inverse Abel transformation[38] or the maximum entropy velocity Legendre reconstruction (MEVELER) method.[39,40] The latter method is used in the present work because it has no center-line-artifact problem. The

photoelectrons with the same velocity form a spherical shell, and the kinetic energy of photoelectrons is given by $E_k = \alpha r^2$, where r is the radius of the photoelectron shell and α is the calibration coefficient. The center position of the peak (r) is given by a Gaussian function fitting. The binding energy (BE) of each transition can be determined by Einstein's equation of photoelectric effect $h\nu = \text{BE} + E_k$, where $h\nu$ is the photon energy.

There are two laser systems used for the photodetachment in the present experiment. One is an optical parametric oscillator (OPO) laser (Spectra-Physics primoScan, 400 – 2700 nm, linewidth ~5 cm^{-1}), and the other is a dye laser (Spectra-Physics, 400–920 nm, linewidth ~0.06 cm^{-1}). The wavelength of the dye laser is monitored by using a wavelength meter (HighFinesse WS6-600) with an accuracy of 0.02 cm^{-1}. Recently, the tuning range of our dye laser has been further extended to the infrared region via a difference frequency generation (DFG) system. The DFG-based infrared laser has a tuning range of 1.5–4.2 μm with a linewidth of 1 cm^{-1}.

TABLE I. Measured binding energies and optimized binding energies of transitions observed in the present work.

Peaks	Levels (Sc$^-$ → Sc)[a]	Measure binding energy (cm^{-1})	Optimized binding energy (cm^{-1})[b]
a	$^3D_1 \to 3d4s^2\,^2D_{3/2}$	313(58)	315.0(28)
b	$^3D_1 \to 3d4s^2\,^2D_{5/2}$	452(58)	483.3(28)
c	$^1D_2 \to 3d4s^2\,^2D_{3/2}$	1 465(53)	1 446.78(18)
d	$^1D_2 \to 3d4s^2\,^2D_{5/2}$	1 630(51)	1 615.12(18)
e	$^3D_1 \to 3d4s(^3D)4p\,^4F^o_{3/2}$	15 992.6(63)	15 987.6(28)
f	$^3D_1 \to 3d4s(^3D)4p\,^4F^o_{5/2}$	16 079.4(68)	16 071.5(28)
h	$^3D_1 \to 3d4s(^3D)4p\,^4D^o_{3/2}$	16 333.6(64)	16 336.8(28)
	$^3D_1 \to 3d4s(^1D)4p\,^2D^o_{5/2}$	16 333.6(64)	16 337.7(28)
i	$^1D_2 \to 3d^2(^3F)4s\,^2F_{5/2}$	16 372.99(95)	16 372.85(18)
j	$^3D_1 \to 3d4s(^1D)4p\,^2D^o_{3/2}$	16 408.6(55)	16 411.9(28)
k	$^1D_2 \to 3d^2(^3F)4s\,^2F_{7/2}$	16 488.70(18)	16 488.70(18)
l	$^1D_2 \to 3d4s(^3D)4p\,^4F^o_{3/2}$	17 119.3(52)	17 119.36(18)
m	$^1D_2 \to 3d4s(^3D)4p\,^4F^o_{5/2}$	17 203.5(51)	17 203.35(18)
n	$^1D_2 \to 3d4s(^3D)4p\,^4D^o_{3/2}$	17 469.4(50)	17 468.60(18)
	$^1D_2 \to 3d4s(^1D)4p\,^2D^o_{5/2}$	17 469.4(50)	17 469.51(18)
o	$^1D_2 \to 3d4s(^1D)4p\,^2D^o_{3/2}$	17 543.4(50)	17 543.68(18)
p	$^1D_2 \to 3d4s(^3D)4p\,^4D^o_{5/2}$	17 588.1(51)	17 587.84(18)

[a]The electronic configuration of Sc$^-$ is $3d4s^24p$, and its parity is odd.
[b]Deduced value according to the assignment, the measured EA value, the measured binding energy of peaks, and the energy levels of the neutral atom Sc.

TABLE II. Summary of the electron affinity value of Sc and an excited state of Sc$^-$.[a]

References	Electron affinity of Sc	Excited state of Sc$^-$
Feigerle et al.[8] (measured)	0.189(20) eV ($^1D^o$ or $^3D^o$)	1190(230) cm^{-1} ($^1D^o$ or $^3D^o$)
Jeung et al.[9] (calculated)	0.14 eV ($^1D^o$)	
Bauschlicher et al.[11] (calculated)	0.195 eV ($^1D^o$)	1480 cm^{-1} ($^3D^o$)
Nobuaki et al.[12] (calculated)	0.181 eV ($^1D^o$)	1060 cm^{-1} ($^3D^o$)
This work(measured)	0.179 378(22) eV or 1446.78(18) cm^{-1} ($^1D^o_2$)	1131.8(28) cm^{-1} ($^3D^o_1$)

[a]The right superscript o of the term symbol indicates the odd parity, which was omitted in the main text for simplicity.
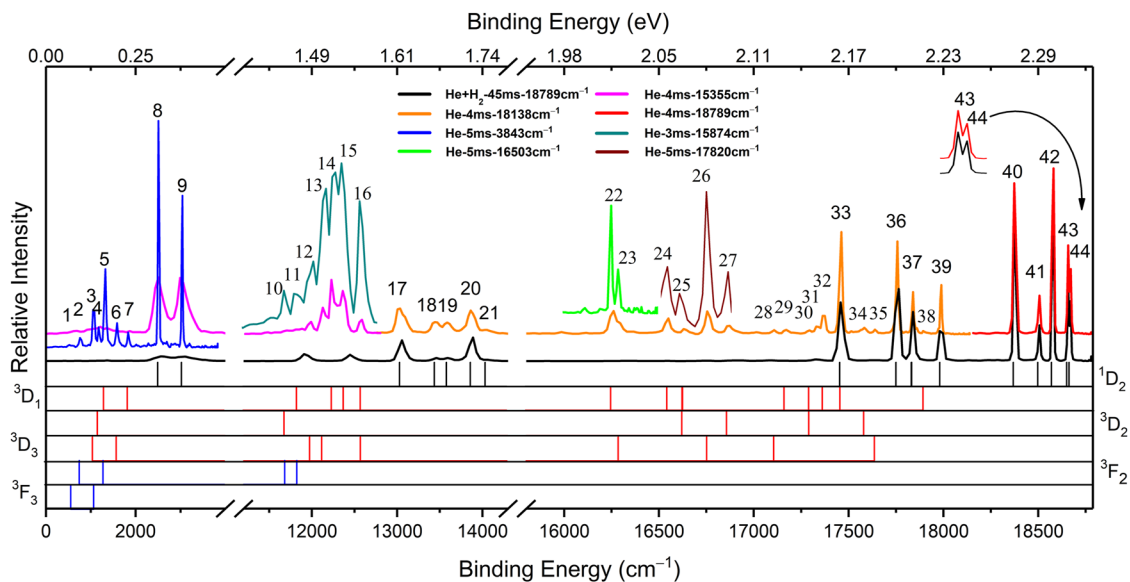
FIG. 6. The photoelectron energy spectra of Y⁻ in the ion-trap-on mode. The Y⁻ ions are trapped for 45 ms with a mixture of 80% He and 20% H_2 as the buffer gas (the black line) or for less than 5 ms with He (the other color lines). There are several sets of sticks below the spectra indicating the energy levels of the final neutral states. The black sticks are for the anionic ground state $^1D_2$, and the other colors are for the excited states ^3D and ^3F.

FIG. 7. The diagram of the observed transitions from the ground state of Y⁻. The ground state of Y is $4d5s^2$ $^2D_{3/2}$, and the ground state is $4d5s^25p$ $^1D_2$ for Y⁻. The transition labels are the same as the indices of measured peaks in Fig. 6. The transitions 33, 36, and 39–44 in red are selected for the electron affinity measurement of Y in the present work.

III. RESULTS AND DISCUSSION

Figure 1 shows the photoelectron imaging and energy spectrum of Sc^- at photon energy 17 912 cm^{-1} in black. It is obtained with the cryogenic ion trap at a temperature of 15 K and a trap time of 5 ms using He as the buffer gas. No contamination from hydrides ScH^- has been observed in the spectrum of Sc^- because our mass spectrometer can separate two species completely. Considering that the atomic energy levels of neutral Sc are well known with high accuracy, these data can be taken as "fingerprints" for the state assignment. Based on the selection rule and the energy levels of neutral Sc atoms,[41] all peaks in Fig. 1 are transitions from the ground state of Sc^-, which is identified as $Sc^-(^1D_2)$. Peak k, which corresponds to the transition from the anionic ground state $Sc^-(^1D_2)$ to the atomic excited state $Sc(^2F_{7/2})$, is selected for the EA measurement of Sc.

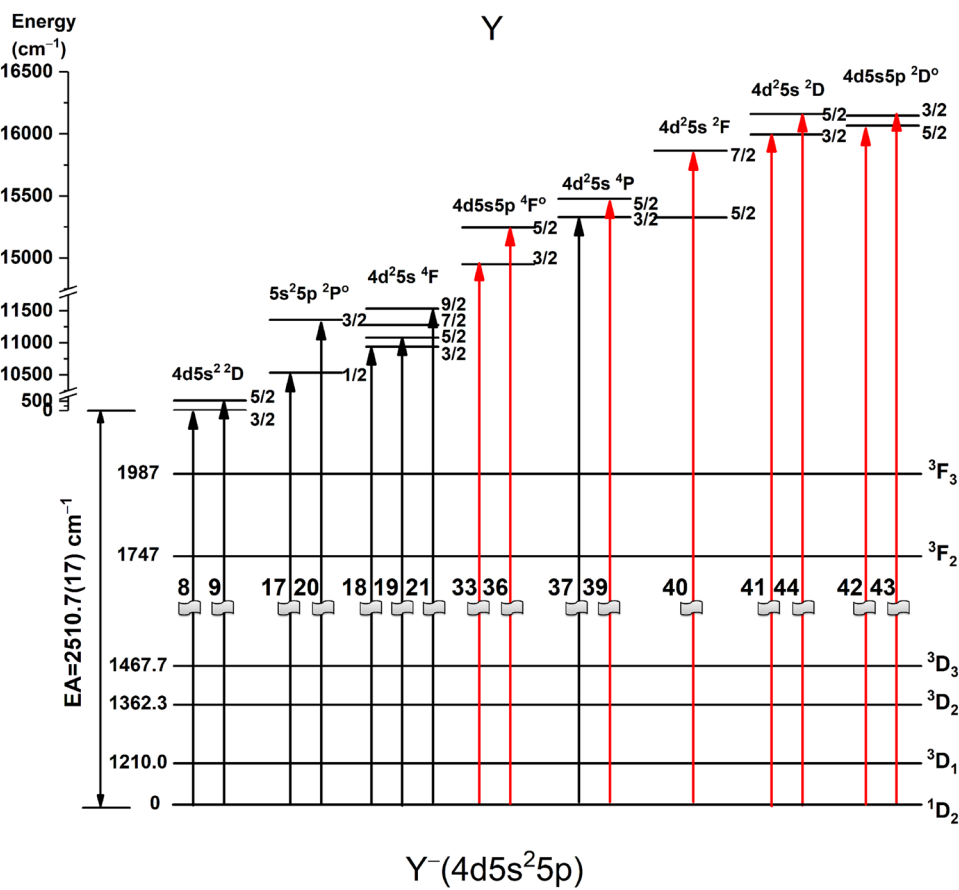For measuring the binding energy of transition k accurately, the photon energy has been scanned slightly above its photodetachment threshold in steps of 10 cm^{-1} from 16 500 cm^{-1} to 16 540 cm^{-1}. Peaks k and i became very sharp at these photon energies, as shown

in Fig. 1 in red. Since the squared radius r^2 of the photoelectron sphere is proportional to its kinetic energy, the experimental data can be fitted as a straight line between $h\nu$ and r^2, as shown in Fig. 2. Based on the equation $h\nu = BE + \alpha r^2$, the binding energy of transition $Sc(^2F_{7/2}) \leftarrow Sc^-(^1D_2)$ is given by the intercept between the fitted line and the vertical axis, which is determined to be 16 488.70 ± 0.18 cm^{-1}. Since the final state $^2F_{7/2}$ has an energy level of 15 041.92 cm^{-1} above the ground state, EA(Sc) is determined to be 1446.78(18) cm^{-1} or 0.179 378(22) eV. The conversion of energy units follows the 2018 CODATA recommendation: 1 eV = 8065.543 937. . . cm^{-1},[43] and the uncertainty of the EA value includes the linewidth of the laser: 0.06 cm^{-1}.

Both peaks i and k are from the ground state of Sc^-. Therefore, the binding energy difference between two peaks equals the energy difference of the final states $Sc(^2F_{7/2})$ and $Sc(^2F_{5/2})$, which is well known to be 115.841(14) cm^{-1} according to the NIST atomic data.[41] As shown in Fig. 3, we determined the binding of the transition i ($^1D_2 \rightarrow {}^2F_{5/2}$) as 16 372.99(95) cm^{-1}. This value is in excellent agreement with the deduced value 16 372.85(18) cm^{-1} according to the NIST atomic data and our measured binding energy of peak k.

FIG. 8. The diagram of the observed transitions from the excited states of Y^-. The transition labels are the same as the indices of measured peaks in Fig. 6.

The deviation is only 0.14 cm^{-1}. This provides another check for the accuracy of our method along with our previous work.[26,42]

To further resolve the excited states of Sc$^-$, we acquired spectra at lower photon energies of 4163 and 4997 cm^{-1}. Figure 4 depicts photoelectron spectra at various photon energies. The spectra in different working modes are pieced together to distinguish the transitions from the different anionic initial states. More peaks are observed by tuning off the ion trap, indicating the short-lived excited states. In this working mode, the Sc$^-$ ions fly from the ion source to the photodetachment zone in a relatively short time of ~100 μs. A comparison of the trapped (lower curves) and the no-trap (upper curves) spectra can tell which peak is from the ground state and which is from the excited state. According to the selection rules of photodetachment and the energy levels of the neutral Sc atom,[41] all new peaks a, b, e, f, h, and j are assigned as the transitions from a common excited state Sc$^-$($^3D_1$) to the different neutral states. Only peak g in Fig. 4 cannot be assigned to a known state, which might be due to an unknown contamination with the same mass as that of Sc. All observed transitions are illustrated in Fig. 5.

The energy level of the anionic excited state $3d4s^24p\ ^3D_1$ can be determined from the binding energy of transitions c, e, f, h, and j. For transition c, its binding energy is just the EA(Sc) value, whereas the binding energies of transitions e, f, h, and j could be given by BE = $h\nu - \alpha r^2$, where the coefficient α has been determined based on the known transitions i and $k - p$. To obtain the interval between these two energy levels, a global optimization analysis based on the covariance algebra has been carried out since multiple transitions are observed in the experiment.[44,45] The measured values of the present work and the neutral Sc energy levels are utilized for the consistent analysis. Eventually, the excited state $3d4s^24p\ ^3D_1$ is determined to be 1131.8(28) cm^{-1} above the ground state $^1D_2$. In Table I, the measured binding energies of observed transitions are compared with the optimized values according to the assignment. The experimental and calculated results for Sc$^-$ are summarized in Table II. Our results agree well with the experimental results by Feigerle et al.[8]

Figure 6 shows the photoelectron energy spectra of Y$^-$ acquired with the ion-trap-on mode. It includes 44 peaks in total. It is the most complicated spectrum that we have observed so far. It should be pointed out that the ion beam Y$^-$ intensity becomes much weaker and the mass resolution becomes worse in the ion-trap-off mode. Therefore, the spectra are acquired only in the ion-trap-on mode. The excited states of Y$^-$ have been distinguished from the ground state by changing the buffer gas and the trap time. There is more chance to observe the excited states with a short trap time using He as buffer gas. All observed peaks can be assigned with six initial states of the atomic anion Y$^-$ except peak 31. Peaks 8, 9, 17–21, 33, 36–37, and 39–44 are from the ground state Y$^-$($^1D_2$) to the different neutral states. After carefully comparing the positions of the peaks with the energy levels of the neutral atom Y, five excited states of Y$^-$ have been eventually identified. Peaks 5, 7, 11, 14–16, 22, 24–25, 29–30, 32–33, and 38 are from the first excited state Y$^-$($^3D_1$). Peaks 4, 10, 25, 27, 30, and 34 are from the second excited state Y$^-$($^3D_2$). Peaks 3, 6, 12–13, 16, 23, 25–26, 28, and 35 are from the third excited state Y$^-$($^3D_3$). Peaks 2, 5, and 10–11 are from the fourth excited state Y$^-$($^3F_2$). Peaks 1 and 3 are from the fifth excited state Y$^-$($^3F_3$). The observed transition diagrams are illustrated in Figs. 7 and 8.

Since Y$^-$ has many excited states and the neutral energy levels are very dense, it will take a much longer time to achieve the same statistic accuracy for each peak as we did for Sc$^-$. Instead of scanning the photon energy slightly above the photodetachment threshold of a certain transition, we choose multiple transitions 33, 36, and 39–44 starting from the ground state of Y$^-$ to measure the electron affinity at one fixed photon energy. This can significantly reduce the total acquisition time. The uncertainty due to the longtime drift is also reduced. Since the difference between the photon energy $h\nu$ and the energy level E_{neu} of Y atom is well known with a high accuracy, the experimental data are plotted as $h\nu - E_{neu}$ vs r^2. As shown in Fig. 9, the electron affinity value is given by the intercept between the fitted line and the vertical axis based on the relation $h\nu - E_{neu} = $ EA $+ \alpha r^2$. Consequently, the EA value of Y is determined to be 2510.7(17) cm^{-1} or 0.311 29(22) eV. The uncertainty has also included the laser linewidth of 0.06 cm^{-1}.

The binding energies of all transitions starting from the ground state of Y$^-$ are known once the EA of Y is accurately determined. These transitions can be used for the energy calibration for later experiments at different conditions to determine the binding energy of the transitions from the excited states of Y$^-$. For example, the fifth excited state Y$^-$($^3F_3$) could be calculated from the binding energies of transitions 1 and 3. The binding energies of observed peaks and their assignment are listed in Table III with a global optimization analysis based on the covariance algebra.[44,45] Note that some of these transitions do not follow the simple single-electron selection rule, which might be due to the strong correlation effect and the strong relativistic effect.
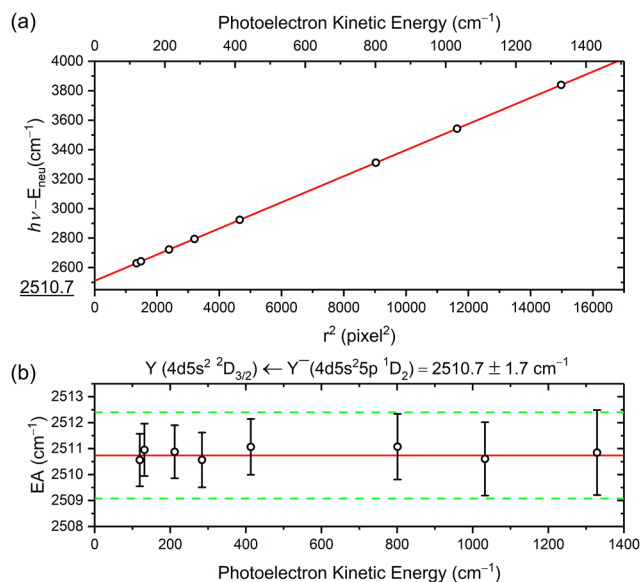
(a)

(b)

FIG. 9. (a) The difference between the photon energy $h\nu$ and the neutral energy level E_{neu} ($h\nu - E_{neu}$) vs the squared radius r^2 of the photoelectron spherical shell. The red solid line is the linear least squares fitting, whose intercept 2510.7(17) cm^{-1} is the EA value of Y. (b) The electron affinity of Y as a function of the photoelectron kinetic energy. The green dashed lines represent $\pm$1.7 cm^{-1} uncertainty.

TABLE III. Measured binding energies and optimized binding energies of transitions observed in the present work.

Peaks	Levels ($\text{Y}^- \to \text{Y}$)[a]	Measured binding energy (cm^{-1})	Optimized binding energy (cm^{-1})[b]
1	$^3F_3 \to 4d5s^2\,^2D_{3/2}$	532(51)	524(33)
2	$^3F_2 \to 4d5s^2\,^2D_{3/2}$	751(47)	763(16)
3	$^3D_3 \to 4d5s^2\,^2D_{3/2}$	1 049(42)	1 043.1(26)
	$^3F_3 \to 4d5s^2\,^2D_{5/2}$	1 049(42)	1 054(33)
4	$^3D_2 \to 4d5s^2\,^2D_{3/2}$	1 165(41)	1 148.4(30)
5	$^3D_1 \to 4d5s^2\,^2D_{3/2}$	1 307(39)	1 300.7(13)
	$^3F_2 \to 4d5s^2\,^2D_{5/2}$	1 307(39)	1 294 (16)
6	$^3D_3 \to 4d5s^2\,^2D_{5/2}$	1 575(35)	1 573.4(26)
7	$^3D_1 \to 4d5s^2\,^2D_{5/2}$	1 829(31)	1 831.1(13)
8	$^1D_2 \to 4d5s^2\,^2D_{3/2}$	2 511(21)	2 510.7(5)
9	$^1D_2 \to 4d5s^2\,^2D_{5/2}$	3 043(13)	3 041.1(5)
10	$^3F_2 \to 4d^2(^3F)5s\,^4F_{3/2}$	11 695(27)	11 701(16)
	$^3D_2 \to 5s^25p\,^2P^o_{1/2}$	11 695(27)	11 677.6(30)
11	$^3F_2 \to 4d^2(^3F)5s\,^4F_{5/2}$	11 845(24)	11 842 (16)
	$^3D_1 \to 5s^25p\,^2P^o_{1/2}$	11 845(24)	11 829.9(13)
12	$^3D_3 \to 4d^2(^3F)5s\,^4F_{3/2}$	11 982(22)	11 980.5(26)
13	$^3D_3 \to 4d^2(^3F)5s\,^4F_{5/2}$	12 134(16)	12 121.7(26)
14	$^3D_1 \to 4d^2(^3F)5s\,^4F_{3/2}$	12 246(15)	12 238.1(13)
15	$^3D_1 \to 4d^2(^3F)5s\,^4F_{5/2}$	12 372(16)	12 379.3(13)
16	$^3D_1 \to 4d^2(^3F)5s\,^4F_{7/2}$	12 579(15)	12 578.7(13)
	$^3D_3 \to 4d^2(^3F)5s\,^4F_{9/2}$	12 579(15)	12 575.2(26)
17	$^1D_2 \to 5s^25p\,^2P^o_{1/2}$	13 042.0(51)	13 039.9(5)
18	$^1D_2 \to 4d^2(^3F)5s\,^4F_{3/2}$	13 449(14)	13 448.1(5)
19	$^1D_2 \to 4d^2(^3F)5s\,^4F_{5/2}$	13 587(15)	13 589.3(5)
20	$^1D_2 \to 5s^25p\,^2P^o_{3/2}$	13 870.0(44)	13 870.5(5)
21	$^1D_2 \to 4d^2(^3F)5s\,^4F_{5/2}$	14 041(15)	14 042.8(5)
22	$^3D_1 \to 4d(^3D)5s5p\,^4F^o_{3/2}$	16 252.8(51)	16 249.7(13)
23	$^3D_3 \to 4d(^3D)5s5p\,^4F^o_{5/2}$	16 291.5(51)	16 288.9(26)
24	$^3D_1 \to 4d(^3D)5s5p\,^4F^o_{5/2}$	16 550.1(59)	16 546.5(13)
25	$^3D_1 \to 4d^2(^3P)5s\,^4P_{3/2}$	16 625.7(83)	16 629.6(13)
	$^3D_1 \to 4d^2(^3F)5s\,^2F_{5/2}$	16 625.7(83)	16 627.5(13)
	$^3D_2 \to 4d^2(^3P)5s\,^4P_{5/2}$	16 625.7(83)	16 625.0(30)
26	$^3D_3 \to 4d(^3D)5s5p\,^4F^o_{7/2}$	16 750.9(51)	16 755.6(26)
27	$^3D_2 \to 4d(^3D)5s5p\,^4F^o_{7/2}$	16 863.7(56)	16 860.9(30)
28	$^3D_3 \to 4d(^3D)5s5p\,^2D^o_{5/2}$	17 109.3(54)	17 109.1(26)
29	$^3D_1 \to 4d^2(^3F)5s\,^2F_{7/2}$	17 163.9(53)	17 165.2(13)
30	$^3D_1 \to 4d^2(^1D)5s\,^2D_{3/2}$	17 294.4(55)	17 294.8(13)
	$^3D_2 \to 4d(^3D)5s5p\,^2D^o_{3/2}$	17 294.4(55)	17 294.6(30)
32	$^3D_1 \to 4d(^3D)5s5p\,^2D^o_{5/2}$	17 370.7(52)	17 366.8(13)
33	$^1D_2 \to 4d(^3D)5s5p\,^4F^o_{3/2}$	17 459.3(16)	17 459.7(5)
	$^3D_1 \to 4d^2(^1D)5s\,^2D_{5/2}$	17 459.3(16)	17 459.6(13)
34	$^3D_2 \to 4d(^3D)5s5p\,^4D^o_{1/2}$	17 580.5(55)	17 584.3(30)
35	$^3D_1 \to 4d(^3D)5s5p\,^4D^o_{3/2}$	17 640.4(52)	17 640.4(26)
36	$^1D_2 \to 4d(^3D)5s5p\,^4F^o_{5/2}$	17 756.0(14)	17 756.5(5)
37	$^1D_2 \to 4d^2(^3P)5s\,^4P_{3/2}$	17 840.1(14)	17 839.6(5)
38	$^3D_1 \to 4d(^3D)5s5p\,^4D^o_{3/2}$	17 894.2(52)	17 898.3(13)
39	$^1D_2 \to 4d^2(^3P)5s\,^4P_{5/2}$	17 987.3(13)	17 987.3(5)
40	$^1D_2 \to 4d^2(^3F)5s\,^2F_{7/2}$	18 375.4(11)	18 375.2(5)

TABLE III. (*Continued*.)

Peaks	Levels ($\mathbf{Y}^- \to \mathbf{Y}$)[a]	Measured binding energy (cm^{-1})	Optimized binding energy (cm^{-1})[b]
41	$^1D_2 \to 4d^2(^1D)5s\ ^2D_{3/2}$	18 504.5(11)	18 504.8(5)
42	$^1D_2 \to 4d(^3D)5s5p\ ^2D^o_{5/2}$	18 576.9(11)	18 576.8(5)
43	$^1D_2 \to 4d(^3D)5s5p\ ^2D^o_{3/2}$	18 657.1(11)	18 656.9(5)
44	$^1D_2 \to 4d^2(^1D)5s\ ^2D_{5/2}$	18 669.5(11)	18 669.6(5)

[a]The electronic configuration of Y$^-$ is $4d5s^25p$, and its parity is odd.
[b]Deduced value according to the assignment, the measured EA value, the measured binding energy of peaks, and the energy levels of the neutral atom Y.

TABLE IV. Summary of the electron affinity value of Y and the excited states of Y$^-$.[a]

References	Electron affinity of Y	Excited states of Y$^-$
Feigerle *et al.*[8] (measured)	0.308(12) eV ($^1D^o$)	1150(220) cm^{-1} ($^3D^o$)
Bauschlicher *et al.*[11] (calculated)	0.389 eV($^1D^o$)	1690 cm^{-1} ($^3F^o$) 2310 cm^{-1} ($^3D^o$)
This work(measured)	0.311 29(22) eV or 2510.7(17) cm^{-1} ($^1D^o_2$)	1210.0(13) cm^{-1} ($^3D^o_1$) 1362.3(30) cm^{-1} ($^3D^o_2$) 1467.7(26) cm^{-1} ($^3D^o_3$) 1747(16) cm^{-1} ($^3F^o_2$) 1987(33) cm^{-1} ($^3F^o_3$)

[a]The right superscript o of the term symbol indicates the odd parity, which was omitted in the main text for simplicity.

Eventually, the first excited state $4d5s^25p\ ^3D_1$ is determined to be 1210.0(13) cm^{-1} above the ground state $^1D_2$, and the energy levels of other four excited states are 1362.3(30) cm^{-1} ($^3D_2$), 1467.7(26) cm^{-1} ($^3D_3$), 1747(16) cm^{-1} ($^3F_2$), and 1987(33) cm^{-1} ($^3F_3$), respectively. The experimental results of ^3D agree well with the work of Feigerle *et al.*[8] Moreover, the energy level ^3F of Y$^-$, which was not observed in the previous works, is observed and measured for the first time. The triplet ^3F state should have three fine-structure states, but only two are observed. It is speculated that $^3F_4$ may be no longer a bound state. Experimental and calculated results for Y$^-$ are summarized in Table IV.

IV. CONCLUSIONS

In conclusion, the electron affinities of Sc and Y are determined to be 1446.78(18) cm^{-1} or 0.179 378(22) eV and 2510.7(17) cm^{-1} or 0.311 29(22) eV, respectively, by using the SEVI method in combination with a cold ion trap. The ground state of Sc$^-$ is identified as $3d4s^24p\ ^1D_2$, and the ground state is $4d5s^25p\ ^1D_2$ for Y$^-$. Additionally, the excited states of their negative ions Sc$^-$ ($^3D_1$) and Y$^-$ ($^3D_1, ^3D_2, ^3D_3, ^3F_2$, and $^3F_3$) are also observed, and their energy levels are accurately measured. The energy levels of the ^3F states of Y$^-$ are measured for the first time. These high-precision experimental results can help people to understand the properties of the transition elements and provide benchmark data for the development of theoretical methods for the strongly correlated system.

AUTHOR DECLARATIONS

Conflict of Interest

The authors have no conflicts to disclose.

Author Contributions

Rui Zhang: Investigation (lead); Writing – original draft (lead); Writing – review & editing (equal). **Yuzhu Lu**: Investigation (supporting). **Rulin Tang**: Investigation (supporting). **Chuangang Ning**: Funding acquisition (lead); Investigation (lead); Supervision (lead); Writing – original draft (supporting); Writing – review & editing (lead).

DATA AVAILABILITY

The data that support the findings of this study are available from the corresponding author upon reasonable request.

REFERENCES

[1] T. Andersen, Phys. Rep. **394**, 157 (2004).
[2] W. C. Lineberger, Annu. Rev. Phys. Chem. **64**, 21 (2013).
[3] T. Andersen, H. K. Haugen, and H. Hotop, J. Phys. Chem. Ref. Data **28**, 1511 (1999).

[4] H. Hotop and W. C. Lineberger, J. Phys. Chem. Ref. Data **4**, 539 (1975).

[5] H. Hotop and W. C. Lineberger, J. Phys. Chem. Ref. Data **14**, 731 (1985).

[6] J. C. Rienstra-Kiracofe et al., Chem. Rev. **102**, 231 (2002).

[7] C. Ning and Y. Lu, J. Phys. Chem. Ref. Data **51**, 021502 (2022).

[8] C. S. Feigerle, Z. Herman, and W. C. Lineberger, J. Electron. Spectros. Relat. Phenom. **23**, 441 (1981).

[9] G. H. Jeung, Phys. Lett. A **113**, 73 (1985).

[10] C. F. Fischer, J. B. Lagowski, and S. H. Vosko, Phys. Rev. Lett. **59**, 2263 (1987).

[11] C. W. Bauschlicher, Jr., S. R. Langhoff, and P. R. Taylor, Chem. Phys. Lett. **158**, 245 (1989).

[12] N. Miura et al., Theor. Chem. Acc. **99**, 248 (1998).

[13] C. Hock et al., J. Chem. Phys. **137**, 244201 (2012).

[14] X.-B. Wang and L.-S. Wang, Rev. Sci. Instrum. **79**, 073108 (2008).

[15] R. Tang, X. Fu, and C. Ning, J. Chem. Phys. **149**, 134304 (2018).

[16] A. Osterwalder et al., J. Chem. Phys. **121**, 6317 (2004).

[17] I. León et al., Rev. Sci. Instrum. **85**, 083106 (2014).

[18] X. Fu et al., J. Chem. Phys. **147**, 064306 (2017).

[19] R.-L. Tang et al., Phys. Rev. A **98**, 020501 (2018).

[20] X. Fu et al., J. Chem. Phys. **145**, 164307 (2016).

[21] Z.-H. Luo et al., Phys. Rev. A **93**, 020501 (2016).

[22] S. Li et al., J. Chem. Phys. **157**, 044302 (2022).

[23] X. Chen and C. Ning, J. Phys. Chem. Lett. **8**, 2735 (2017).

[24] X. Chen et al., Sci. Rep. **6**, 24996 (2016).

[25] X.-L. Chen and C.-G. Ning, Phys. Rev. A **93**, 052508 (2016).

[26] L. Lu et al., J. Chem. Phys. **152**, 034302 (2020).

[27] R. Tang et al., J. Phys. Chem. Lett. **10**, 702 (2019).

[28] Y. Lu et al., Phys. Rev. A **99**, 062507 (2019).

[29] X.-X. Fu et al., Chin. Phys. B **29**, 073201 (2020).

[30] X.-X. Fu et al., Phys. Rev. A **101**, 022502 (2020).

[31] X.-X. Fu et al., Chin. J. Chem. Phys. **32**, 187 (2019).

[32] R. Tang et al., Phys. Rev. Lett. **123**, 203002 (2019).

[33] R. Tang et al., Phys. Rev. A **103**, 042817 (2021).

[34] R. Tang et al., Phys. Rev. A **103**, L050801 (2021).

[35] J. B. Kim, M. L. Weichman, and D. M. Neumark, Mol. Phys. **113**, 2105 (2015).

[36] W. C. Wiley and I. H. McLaren, Rev. Sci. Instrum. **26**, 1150 (1955).

[37] A. T. J. B. Eppink and D. H. Parker, Rev. Sci. Instrum. **68**, 3477 (1997).

[38] V. Dribinski et al., Rev. Sci. Instrum. **73**, 2634 (2002).

[39] B. Dick, Phys. Chem. Chem. Phys. **16**, 570 (2014).

[40] B. Dick, Phys. Chem. Chem. Phys. **21**, 19499 (2019).

[41] J. E. Sansonetti and W. C. Martin, J. Phys. Chem. Ref. Data **34**, 1559 (2005).

[42] R. Tang, X. Fu, Y. Lu, and C. Ning, J. Chem. Phys. **152**, 114303 (2020).

[43] E. Tiesinga et al., Rev. Mod. Phys. **93**, 025010 (2021).

[44] L. J. Radziemski et al., Comput. Phys. Commun. **3**, 9 (1972).

[45] A. E. Kramida, Comput. Phys. Commun. **182**, 419 (2011).